CHEMISTRY OF MATERIALS
Article

Chem. Mater. **2010,** *22,* 5279–5289 5279
DOI:10.1021/cm101429u

Structural and Mechanistic Studies of the Dehydration of $MoO_2PO_3OH \cdot H_2O$ and the In situ Identification of Two New Molybdenum Phosphates

Sarah E. Lister, Victoria J. Rixom, and John S. O. Evans*

Department of Chemistry, Durham University, Science Laboratories, South Road, Durham DH1 3LE, United Kingdom

Received May 21, 2010. Revised Manuscript Received July 26, 2010

We report investigations into the dehydration pathway of the precursor material $MoO_2PO_3OH \cdot H_2O$ to γ-$(MoO_2)_2P_2O_7$. The reaction occurs in three distinct stages via the formation of two new previously unidentified molybdenum phosphate phases, β-$MoOPO_4$ and δ-$(MoO_2)_2P_2O_7$. Conditions for the isolation of these phases were identified by a whole powder pattern fitting technique to follow phase evolution versus time and temperature and later verified by full Rietveld refinement. Structural refinement of β-$MoOPO_4$ was performed against X-ray and neutron data. The new phase has lattice parameters $a = 7.4043(3)$ Å, $b = 7.2128(3)$ Å, $c = 7.2876(3)$ Å, $\beta = 118.346(2)°$, and volume 342.53(3) Å^3 at room temperature, containing 7 unique atoms in space group Cc. δ-$(MoO_2)_2P_2O_7$ forms on slowly heating the precursor material to 793 K. Lattice parameters at room temperature are $a = 16.2213(11)$ Å, $b = 3.8936(3)$ Å, and $c = 6.2772(4)$ Å and volume 396.46(5) Å^3, in space group $C222_1$. A transformation mechanism is proposed for the dehydration. Lithium intercalation into layered δ-$(MoO_2)_2P_2O_7$ has been shown.

Introduction

The use of chimie douce methods to target metastable compounds has opened up a vast field in chemical synthesis providing a route to many new and important materials.[1,2] Low-temperature hydrothermal routes to metastable zeolites provide one example. Specific metastable materials can also be targeted using topotactic reactions, in which the crystal structure of a precursor phase leads to the formation of a product with a particular structure.[3] Examples include routes to potential Li-battery materials like $LiMnO_2$,[4,5] VS_2,[6,7] and λ-MnO_2[8] using cationic exchange and lithium extraction methods.

We present here investigations into the dehydration pathway of $MoO_2PO_3OH \cdot H_2O$, prepared originally as a precursor for the synthesis of α-/γ-$(MoO_2)_2P_2O_7$.[9,10] This latter material undergoes two displacive structural phase transitions on cooling from the high-temperature γ-form to a complex low-temperature α-superstructure via an incommensurate β-form; the phase will be referred to as γ-$(MoO_2)_2P_2O_7$ throughout this paper as all our refinements use the simple high-temperature structure.[10] $MoO_2PO_3OH \cdot H_2O$ was first isolated by Schulz in 1955;[11] its structure was reported by Kierkegaard as $Mo(OH)_3PO_4$ in the monoclinic space group $P2_1/m$,[12] and can be described as containing corner-sharing MoO_6 octahedra and PO_4 tetrahedra. The structure contains chains of alternating P and Mo polyhedra along [010] as pictured in Figure 1. Later structural investigations by Weller et al. and Biot et al. used powder neutron and X-ray studies, respectively, to accurately locate the H atom positions and determine the molecular assignment as $MoO_2PO_3OH \cdot H_2O$.[13,14] Previous investigations into the dehydration of this material using XRD, TGA and IR spectroscopic techniques failed to clarify its transformation.[15,16] We describe here our results using in situ diffraction data, which rely on a method of quantitative phase analysis similar to that described by Scarlett and Madsen.[17] The phase evolution is monitored quantitatively without knowledge of either the unit cell or structure of the unknown materials. This analysis allowed optimal conditions for the isolation of two new phases whose

*To whom all correspondence should be addressed. E-mail: john.evans@durham.ac.uk.

(1) Gopalakrishnan, J. *Chem. Mater.* **1995**, *7*, 1265–1275.
(2) Rouxel, J.; Tournoux, M. *Solid State Ionics* **1996**, *84*, 141–149.
(3) Lotgering, F. K. *J. Inorg. Nucl. Chem.* **1959**, *9*, 113–123.
(4) Armstrong, A. R.; Bruce, P. G. *Nature* **1996**, *381*, 499–500.
(5) Capitaine, F. C.; Gravereau, P.; Delmas, C. *Solid State Ionics* **1996**, *89*, 197–202.
(6) Murphy, D. W.; Cros, C.; DiSalvo, F. J.; Waszczak, J. V. *Inorg. Chem.* **1977**, *16*, 3027–31.
(7) Murphy, D. W.; Carides, J. N.; diSalvo, F. J.; Cros, C.; Waszczak, J. V. *Mater. Res. Bull.* **1977**, *12*, 825–830.
(8) Hunter, J. C. *J. Solid State Chem.* **1981**, *39*, 142–147.
(9) Kierkegaard, P. *Ark. Kemi* **1962**, *19*, 1–14.
(10) Lister, S. E.; Soleilhavoup, A.; Withers, R. L.; Hodgkinson, P.; Evans, J. S. O. *Inorg. Chem.* **2010**, *49*, 2290–2301.
(11) Schulz, I. *Z. Anorg. Allg. Chem.* **1955**, *281*, 99–112.
(12) Kierkegaard, P. *Acta Chem. Scand.* **1958**, *12*, 1701–1714.
(13) Weller, M. T.; Bell, R. G. *Solid State Ionics* **1989**, *35*, 79–84.
(14) Biot, C.; Leclaire, A.; Borel, M. M.; Raveau, B. *Z. Kristallogr.* **1997**, *212*, 792–794.
(15) Glemser, O. *Angew. Chem.* **1961**, *73*, 785–805.
(16) Glemser, O.; Hofmeister, H. K.; Schwarzmann, E. *Z. Anorg. Allg. Chem.* **1960**, *312*, 50–52.
(17) Scarlett, N. V. Y.; Madsen, I. C. *Powder Diffr.* **2006**, *21*, 278–284.

© 2010 American Chemical Society
Published on Web 08/12/2010

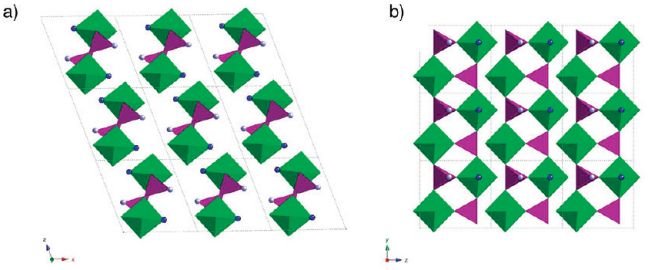

Figure 1. Structure of $MoO_2PO_3OH \cdot H_2O$. $MoO_5 \cdot H_2O$ octahedra are shown in green, the H_2O oxygen is marked in blue, PO_3OH tetrahedra are shown in purple, with the OH oxygen marked in gray. (a) View along [010] shows polyhedral chains in the structure which are held together by H bonding, and (b) the *bc* plane with alternating MoO_6 octahedra and PO_4 tetrahedra forming infinite chains in the [010] direction.

structures could then be solved. These phases appear to form under topotactic control and a mechanistic pathway for the topotactic transformation is also described. One of the new phases, a layered form of $(MoO_2)_2P_2O_7$, has been shown to undergo Li intercalation.

Experimental Section

The white Mo(VI) containing precursor material $MoO_2PO_3OH \cdot H_2O$ was prepared using two different routes. The first, a solution state route, led to a phase pure product.[12] A typical synthesis involved dissolving 7.5 g of MoO_3 (52 mmol, Alfa Aesar, 99.95% metals basis) in 22.5 cm^3 85% H_3PO_4 (331 mmol, Aldrich) at approximately 453 K. The solution was then cooled to room temperature and 200 cm^3 15.8 M HNO_3 (Fisher) added and the solution refluxed for 12 h. On cooling, small crystallites of the target compound precipitated from the solution. These crystals were vacuum-filtered, washed with acetone and left to dry in air. The second method employed a hydrothermal synthesis,[14] typically involving heating 2.48 g MoO_3 (17 mmol, Alfa Aesar, 99.95% metals basis) with 1.77 cm^3 H_3PO_4 (26 mmol, Aldrich) in a Teflon-lined autoclave at 453 K for 12 h. The resulting solid was washed with demineralised water and dried in air. Samples prepared using this method contained approximately 5−15 wt % of MoO_3 by Rietveld analysis. Successful syntheses were confirmed by comparison of the PXRD patterns with the PDF (11−0333).[18]

Variable-temperature X-ray diffraction data were collected on this material using a Bruker D8 diffractometer. The system was equipped with a Ge(111) monochromator giving Cu $K\alpha_1$ (λ = 1.540598 Å) radiation and a Vantec linear PSD detector. Data were collected from 300 to 1023 K using an Anton-Paar HTK1200 furnace. Visual inspection of these data suggested the presence of two new, previously unknown crystalline materials, discussed here as β-$MoOPO_4$ and δ-$(MoO_2)_2P_2O_7$. Whole powder pattern data analysis including these phases prior to structure solution facilitated their synthesis both in situ and ex situ for further investigation. The intensity of each individual peak in the powder data was integrated and their temperature evolution allowed them to be assigned to different phases. This method was later verified using full Rietveld analysis. Further details of these analyses are given in the discussion; refined parameters are listed in the Supporting Information. All crystallographic calculations and refinements were performed using the Topas Academic suite unless specifically stated otherwise.[19]

Blue β-$MoOPO_4$ was isolated by heating the precursor material at 553 K for 60 min and cooling in the furnace to room temperature. Pale gray δ-$(MoO_2)_2P_2O_7$ was synthesized by heating the precursor material to 793 K at a rate of 0.33 K/hour, holding at this temperature for 0.1 h and cooling to room temperature in the furnace. γ-$(MoO_2)_2P_2O_7$ was prepared by heating the precursor material at 923 K for 48 h.

X-ray diffraction data for refinement of β-$MoOPO_4$ at room temperature were obtained in both transmission and reflection geometries using a Siemens D5000 diffractometer equipped with a Ge(111) monochromator and a Braun PSD-50 M linear position sensitive detector and a Bruker D8 diffractometer with Cu $K\alpha_{1,2}$ (λ = 1.54187 Å) radiation and a Lynxeye psd. Time of flight neutron data were recorded on the GEM beamline at the ISIS neutron source of the Rutherford Appleton Laboratory, UK. Data were collected at ambient temperature for 350 μAhrs and analyzed over the *d*-spacing range 0.4−4 Å. In final cycles of refinement a total of 210 parameters were refined for the 5 data sets used, of which 30 were used to describe the structure; these are detailed in the Supporting Information. The final overall R_{wp} for the refinement was 1.85%.

The amount of the amorphous/crystalline phases present within these samples was quantified using the structural model for β-$MoOPO_4$ described in this paper. A β-$MoOPO_4$/MoO_3 sample was "spiked" with known masses of anatase (10, 25, 50 and 75% anatase by mass) and each twice prepared and scanned under identical conditions. The analyzed weight percentages from Rietveld analysis were then scaled from knowledge of the known added mass of crystalline anatase. The amorphous phase percentage could then be extracted by extrapolation. Calculated percentages for the pure sample (extrapolated to 0% anatase) were 12% β-$MoOPO_4$, 15% MoO_3 and 73% amorphous content. These are estimated to be accurate within ±5%. Further information is given in the Supporting Information, Figure S1.

X-ray diffraction data for structure solution and refinement of δ-$(MoO_2)_2P_2O_7$ were recorded at the ESRF on beamline ID31. Data were recorded over two 2θ ranges (0−35 and 10−35°) using a wavelength of 0.35285(8) Å and then normalized and summed to achieve better statistics at shorter *d*-spacings. Time-of-flight data were recorded on HRPD at the ISIS pulsed neutron source of the Rutherford Appleton Laboratory, UK. For final cycles of refinement of δ-$(MoO_2)_2P_2O_7$ 1 X-ray and 2 TOF neutron data sets were refined simultaneously; a total of 111 parameters were refined (21 structural), these are detailed in the Supporting Information. A final agreement factor of R_{wp} = 4.21% (all data sets) was obtained (5.04/3.79/8.37% for 168/90° neutron banks and X-ray data, respectively. Bragg R-factors were 1.44(337)/1.75(146)/5.78(247)%, where the value in parentheses is the number of reflections in each of the three data sets.

Infrared (IR) spectra were recorded on a Perkin-Elmer Spectrum 100 FTIR instrument over the range 450−4000 cm^{-1} using the KBr disk method. TGA was carried out using a Perkin-Elmer Pyris 1 Thermogravimetric Analyzer.

γ- and δ-$(MoO_2)_2P_2O_7$ were intercalated with Li using ^{n}BuLi in hexane under a N_2 atmosphere at room temperature and the mixture was stirred for ten minutes under N_2 flow. A color change from light gray to black was noted for each material. Excess liquid was decanted off and the powders washed then dried. The resulting powders had their X-ray diffraction patterns recorded several times over the period of a few days and showed moderate stability in air. Room temperature X-ray diffraction data were collected on the intercalated material for

(18) *Powder Diffraction File*; International Centre for Diffraction Data: Newtown Square, PA: 1998.
(19) Coelho, A. A. *TOPAS Academic: General Profile and Structure Analysis Software for Powder Diffraction Data*;Bruker AXS: Karlsruhe, Germany, 2004.

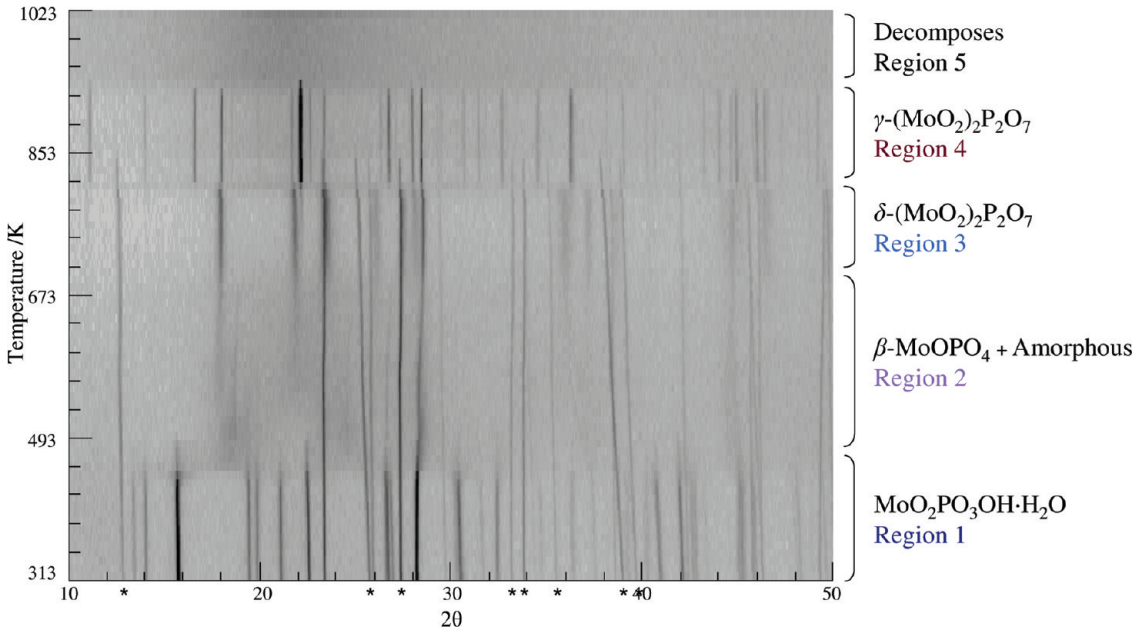

Figure 2. Two-dimensional film representation of powder diffraction data recorded during the dehydration of $MoO_2PO_3OH \cdot H_2O$ on heating from 303 to 1023 K in 10 K steps. A 15% MoO_3 impurity is present up to 853 K; these peaks are denoted with a *. One scan from each of the first four regions is given in the Supporting Information, Figure S2.

structural refinement. Data were recorded over 5−90° 2θ for 12 h. During the final Rietveld refinement a total of 70 parameters were refined; these are detailed in the Supporting Information.

Ion beam analysis was performed on several samples of intercalated δ-$(MoO_2)_2P_2O_7$. Samples were irradiated with 5 μC of 2.50 MeV $^1H^+$ ions, and the nuclear reaction between these incident ions and ^{7}Li in the sample was used to determine the Li content. The nuclear reaction generates energetic alpha particles according to:

$$^1H + {}^7Li \rightarrow 2{}^4He + 17.347MeV$$

Backscattered ^{4}He was detected using a 300 μm SSB detector at 150° to the incident beam. Only recoils with energy greater than 5 MeV were used to calculate the Li content, because at this energy there is negligible background due to pile-up of elastically recoiled particles. The integrated spectrum was compared with a quantitative simulation using SIMNRA version 5.02.[20]

Results and Discussion

Dehydration of $MoO_2PO_3OH \cdot H_2O$. In situ XRD studies on $MoO_2PO_3OH \cdot H_2O$ reveal the dehydration reaction occurs in three distinct stages, Figure 2. On heating to 423 K, the Bragg peaks of the precursor disappear, a sharp increase in background intensity occurs and, following the complete disappearance of the precursor phase, a new set of weak peaks arise, which we show later are due to a new poorly crystalline phase, β-$MoOPO_4$. On further heating above 700 K these peaks are replaced by those of a second unknown intermediate phase (later shown to be δ-$(MoO_2)_2P_2O_7$), before formation of the known, fully dehydrated phase, γ-$(MoO_2)_2P_2O_7$, above 773 K. Neither of the intermediate diffraction patterns matched a known Mo/P/O/H containing phase.

Quantitative analysis to identify the optimal ex situ synthetic conditions to prepare single phase samples of each of the new phases was performed from a similar experiment in which a sample of the hydrated precursor was heated stepwise to 793 K and repeated scans recorded at that temperature. Because neither cell parameters nor structures of intermediate phases were known, quantification could not be performed using either Pawley fitting or Rietveld analysis. Each Bragg intensity was therefore determined individually as a function of temperature using Topas Academic.[19] It was then possible to assign reflections to different phases from their different temperature evolution and sum the total Bragg intensity arising from each unknown phase as a function of temperature. A similar description was used to model the significant increase in background intensity arising because of the formation of an amorphous component following the initial dehydration at 423 K (region 2). This amorphous intensity is plotted in Figure 3a, but is not included in the summation (Total Intensity) for ease of comparison with Figure 3b, discussed later. Calculated percentages of one sample of the material from region 2 were 12% β-$MoOPO_4$, 15% MoO_3, and 73% amorphous content. These are estimated to be accurate within ±5%.

The known phases, $MoO_2PO_3OH \cdot H_2O$, γ-$(MoO_2)_2P_2O_7$ (subcell model), and a small quantity of an MoO_3 impurity phase were modeled using Rietveld analysis. For direct comparison with the unknown phases the total peak intensities due to these phases in each scan were calculated and used to place the Rietveld scale factor on the same scale as the observed intensities of the unknown phases. This allowed the quantitative analysis shown in Figure 3a without knowledge of the structures of two of the phases. This information subsequently enabled successful ex situ syntheses of each material, allowing structure solution of each new phase.

(20) Mayer, M. *SIMNRA User's Guide, Report IPP 9/113*; Max-Planck-Institut für Plasmaphysik: Garching, 1997.

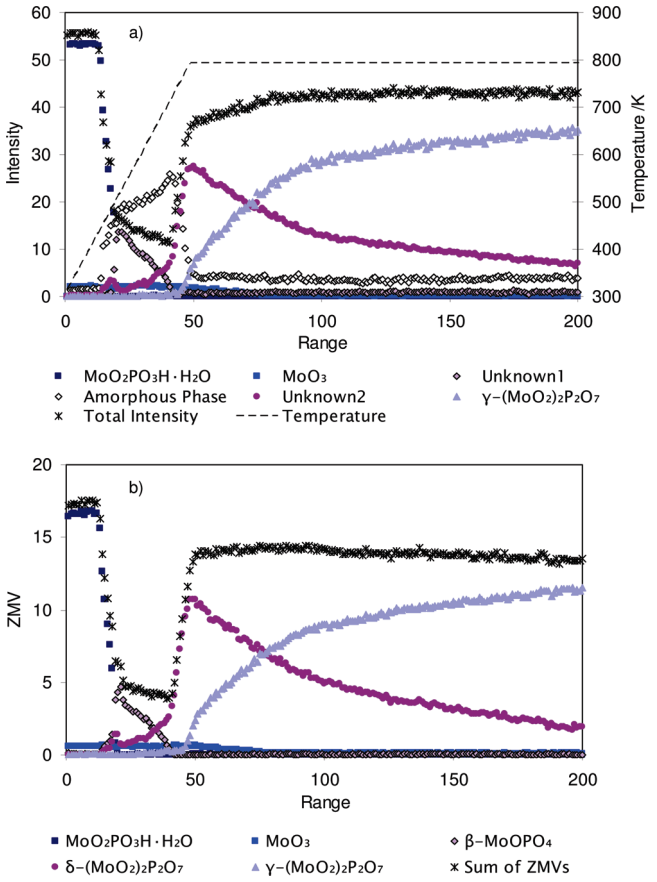

Figure 3. Progress of the dehydration from the starting hydrate, $MoO_2PO_3OH \cdot H_2O$ (with 4% MoO_3 impurity), to β-$MoOPO_4$ and ~70% amorphous phase, through to δ-$(MoO_2)_2P_2O_7$, and finally to γ-$(MoO_2)_2P_2O_7$. Scans were recorded for 30 min every 10 K from 313 to 793 K (ranges 1−49) and then 150 scans were recorded while the temperature was held at 793 K. Analysis results from these data are shown using (a) the structure independent whole powder pattern technique and (b) Rietveld refinement following structural solution of each phase. Results are plotted as ZMV (Rietveld scale factor × number of formula units per unit cell × molar mass × volume) to allow for absolute intensity comparison between the different phases.

Scheme 1

$$MoO_2PO_3OH{\cdot}H_2O \xrightarrow{423\ K} \beta\text{-}MoOPO_4 + \text{amorphous material} \xrightarrow{700\ K} \delta\text{-}(MoO_2)_2P_2O_7 \xrightarrow{773\ K} \gamma\text{-}(MoO_2)_2P_2O_7$$

Region 1 Region 2 Region 3 Region 4

Figure 3b contains comparable results from the equivalent Rietveld-only analysis performed following structure solution of the two unknown phases. This analysis proves the validity of the method used and will be discussed in more detail later. Similar results for a heat/hold reaction with a constant final temperature of 773 K are given in the Supporting Information, Figure S3.

The investigation into the dehydration reaction of $MoO_2PO_3OH \cdot H_2O$ has led to the discovery of two new phases, identified optimal synthetic conditions for the isolation of each of the phases and suggests the reaction proceeds as summarized in Scheme 1. These conclusions are derived primarily from the information available from the crystalline Bragg peaks for each of these phases. We will discuss the nature of the amorphous material later, but speculate here that the material has approximate composition MoO_2PO_3OH.

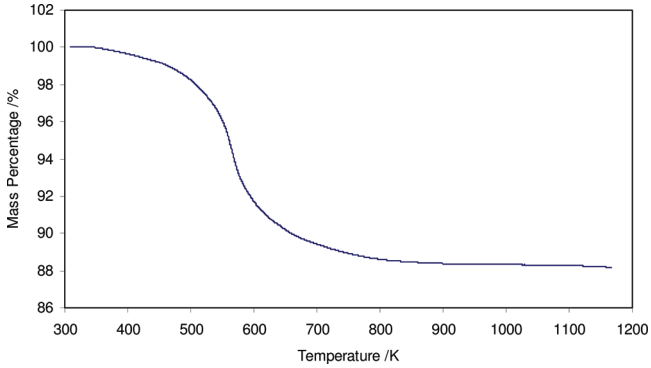

Figure 4. TGA trace recorded on 17.3 mg $MoO_2PO_3OH \cdot H_2O$. Total mass loss 11.7(5)% corresponds to the loss of 1.5 molecules of H_2O per formula unit (calculated loss of 11.2%). The material was heated at 10 K/min from 300 to 1173 K.

The disappearance of water and hydroxyl groups during Scheme 1 was also investigated using thermogravimetry. A gradual mass loss of 11.7(5) % was observed between 400 and 700 K, Figure 4, which corresponds to region 2 of Figure 2; the calculated loss for 1.5 mols of water (per formula unit) is 11.2%. XRD data show β-$MoOPO_4$ begins to form at 423 K, transforming to δ-$(MoO_2)_2P_2O_7$ above 700 K. This implies δ-$(MoO_2)_2P_2O_7$ is free from H_2O or OH and has an empirical formula identical to that of the final phase, $(MoO_2)_2P_2O_7$. IR spectra for each of the four materials are consistent with these conclusions; they are given in Figure S4 in the Supporting Information. A sharp peak arising at 1400 cm^{-1} in the spectra of $MoO_2PO_3OH \cdot H_2O$ and β-$MoOPO_4$/amorphous mixture (and absent in the spectra of δ-$(MoO_2)_2P_2O_7$ and γ-$(MoO_2)_2P_2O_7$) has been assigned to be a P−OH deformation.[21] The presence of an OH group in the spectra of the β-$MoOPO_4$/amorphous mixture is presumably due to the OH groups in the amorphous component.

Full Rietveld Analysis of the Data. Following the structure solution of the unknown phases, full Rietveld analysis of the variable-temperature data was undertaken to compare the results obtained from this method with those based on the intensity fitting. A five phase Rietveld refinement was performed; full details of the refined parameters are given in the Supporting Information. Results from this quantitative phase analysis are given in Figure 3b. They are plotted as Rietveld scale factor × number of formula units per unit cell × molar mass × volume, or ZMV, allowing for absolute intensity comparison between the different phases. The results confirm the conclusions from our structure-independent method. We note that a small loss of absolute ZMV from the hydrated precursor to the final γ-$(MoO_2)_2P_2O_7$ phase is expected because of the loss of water on dehydration. We also note that although the ZMV of β-$MoOPO_4$ falls steadily over the range 23−41, the overall ZMV decreases much more slowly. This suggests that there is a direct transformation between β-$MoOPO_4$ and δ-$(MoO_2)_2P_2O_7$; the rate at which the former material is disappearing is approximately matched by the formation of the latter. The large increase in δ-$(MoO_2)_2P_2O_7$ present after range 41 is due

(21) Corbridge, D. E. C.; Lowe, E. J. *J. Chem. Soc.* **1954**, 4555–4564.

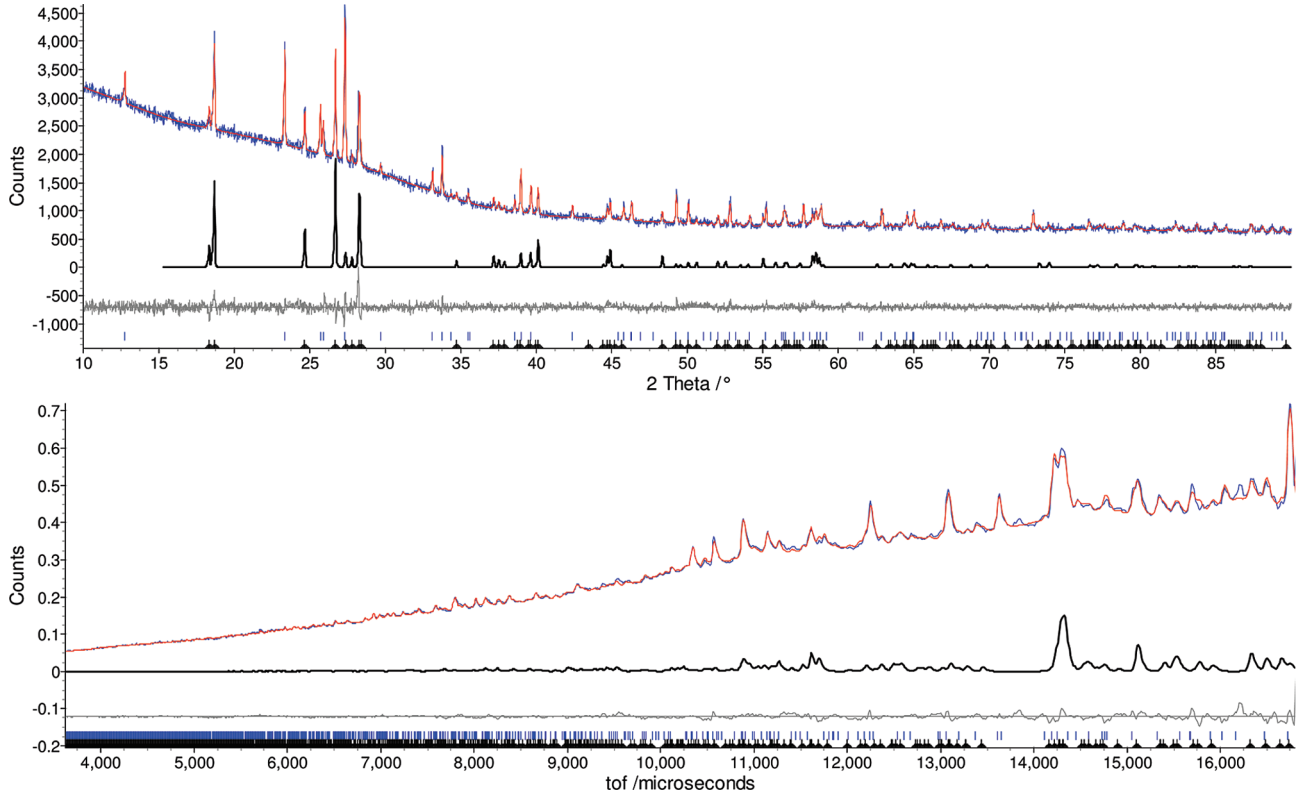

Figure 5. Rietveld fits of β-$MoOPO_4$, against (a) capillary X-ray data and (b) TOF neutron data. The final overall R_{wp} for these refinements was 1.85%. The peak present at 16 200 μs is believed to arise from an impurity phase present. The figure shows experimental data in blue, calculated pattern in red, and difference plot in gray. The contribution of β-$MoOPO_4$ to each pattern is shown in black.

to the crystallization of the significant quantity of amorphous component (as quantified in Figure 3a).

Structure Determination of β-$MoOPO_4$. Ex situ synthesis of the crystalline phase β-$MoOPO_4$ was achieved using conditions derived from Figure 3a. The most crystalline samples could be produced from MoO_2-$PO_3OH \cdot H_2O$ preparations with an initial ~5% MoO_3 impurity; a large amorphous component was always present. Indexing was performed on capillary data to a monoclinic cell with lattice parameters a = 7.4077 Å, b = 7.2128 Å, c = 7.2805 Å, and β = 61.651°. A search of the ICSD[22] revealed a similar cell for ε-$VOPO_4$ in space group Cc.[23] This space group assignment agreed with the observed reflection conditions. The atomic coordinates of ε-$VOPO_4$ were therefore used as starting coordinates. Structural refinement was performed using a combination of reflection and transmission X-ray data and time-of-flight neutron data recorded on the GEM diffractometer at the pulsed ISIS source. Bond length and angle restraints were applied to maintain the atomic connectivity present because of the low-quality of the data available on this poorly crystalline phase. Mo−O bonds were restrained to be 1.9 ± 0.3 Å and P−O bonds were restrained to be 1.52 Å to maintain sensible BVS values at each metal center. Final overall R-factors were R_{wp} 1.85% and goodness of fit 1.898. Final Rietveld fits to the capillary and neutron backscattering data are given in Figure 5; the remaining Rietveld fits are given in the Supporting Information, Figure S5. Selected refinement details are given in Table 1. Despite the crystallinity being low and there being additional minor impurities in the large sample prepared for neutron diffraction studies, we believe the refinement is sufficient to identify the basic structure of transient β-$MoOPO_4$.

Table 1. Selected Refined Values and Crystallographic and Data Collection Parameters for the Combined X-ray and Neutron Refinement of β-$MoOPO_4$

space group	Cc	overall R_{wp} (%)	1.85
a (Å)	7.4043(3)	X-ray transmission R_{wp}/R_{Bragg} (%)	3.49/2.68
b (Å)	7.2128(3)	X-ray reflection R_{wp}/R_{Bragg} (%)	2.00/0.68
c (Å)	7.2876(3)	neutron R_{wp}/R_{Bragg} (%)	1.44/1.03
β (deg)	118.35(1)	GOF	1.90
volume (Å^3)	342.53(3)	no. of params	210

This structure is formed by complete dehydration of the precursor phase $MoO_2PO_3OH \cdot H_2O$ with cross-linking of the 1D chains to form a 3D structure in which MoO_6 octahedra and PO_4 tetrahedra are fully corner-linked. The mechanism of the dehydration is discussed in more detail later. The structure of β-$MoOPO_4$ contains chains of trans- corner-sharing MoO_6 octahedra parallel to [101], with a characteristic long−short alternation of Mo−O bonds along the chain direction. MoO_6 octahedra tilt away from the chain direction due to the formation of Mo−O−P bonds from adjacent octahedra with the same (approximately) regular tetrahedron. The remaining two corners of the PO_4 tetrahedra are linked to two other chains. In the model reported the O−Mo=O bonds in

(22) *ICSD v 2008/2*; Fachinformationszentrum and NIST: Karlsruhe, Germany, and Gaithersburg, MD, 2008.
(23) Girgsdies, F.; Dong, W.-S.; Bartley, J. K.; Hutchings, G. J.; Schlögl, R.; Ressler, T. *Solid State Sci.* **2006**, *8*, 807–812.

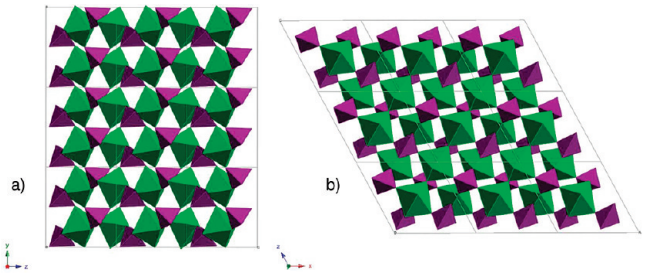

Figure 6. Structure of β-$MoOPO_4$ with MoO_6 octahedra shown in green, PO_4 groups in purple. (a) Connectivity of the PO_4 groups in the *bc* plane. (b) MoO_6 chains along the [101] direction.

parallel chains all point in the same direction. Two views of the structure are given in Figure 6; bond lengths are reported in Table 2; full structural details are given in Supporting Information in CIF format.

The crystal chemistry of $XOPO_4$ materials is complex. Many structural types are known to exist with a rich number of modifications and phase transitions. α-$MoOPO_4$ is known in the literature, crystallizes in the tetragonal space group, $P4/n$,[26] and is isostructural with α-$NbOPO_4$.[27] α-$MoOPO_4$ also contains chains of MoO_6 octahedra joined together through trans linkages (along the *c*-axis).[27,28] though the 3D structure of the material is created by each PO_4 tetrahedron corner sharing with four different chains within the material. In β-$MoOPO_4$, the PO_4 groups link to only three different chains, giving rise to the distinct structure reported here.

The chemistry of the related vanadium phases are of interest because of their use as catalysts and lithium battery materials. There are many known polymorphs of $VOPO_4$; some are known to exhibit only very minor crystallographic differences. For example the α_I- and α_{II}-$VOPO_4$ structures differ in the parallel and antiparallel adjacent chains of O−V═O groups[29] and can be interconverted by a small displacement of the V atom in the distorted octahedra. Lithium insertion into both species, for example, yields a tetragonal phase, $LiVOPO_4$ with the α_I- type lattice.[30]

While the structure we report here is polar with all short Mo−O bonds aligned, we note that two papers have been published on the structure of ε-$VOPO_4$ in the space groups centrosymmetric $P2_1/n$[31] and polar *Cc*;[23] only the latter model contained full structural details and has been used here. It would be hard to distinguish between the two possible models for β-$MoOPO_4$ with the data quality available. We note that attempts to prepare this phase from pure samples of the hydrated precursor led to a less crystalline sample of this minority phase, with only two peaks (the $20\overline{2}$ and $40\overline{4}$ reflections) typically discernible above the background in an XRD pattern. This could be due to the presence of the MoO_3 impurity phase or differences in particle morphology, which can often influence kinetically controlled transformations. Complete dehydration of such samples followed the same sequence of transitions, with the β-$MoOPO_4$ identified from its two main reflections only.

Table 2. Bond Lengths and Bond Valence Sum Values Calculated for β-$MoOPO_4$. BVSs were Calculated Using R_{ij}[Mo(V)] = 1.8790 Å,[24] R_{ij}[P(V)] = 1.604 Å, and b = 0.37 Å[25]

central atom	apex atom	bond length (Å)	BVS (vu)
Mo1	O1	1.877(12)	4.92
	O2	2.125(11)	
	O3	2.032(10)	
	O4	2.011(10)	
	O5	1.812(11)	
	O1	2.062(11)	
P1	O2	1.505(11)	4.92
	O3	1.564(13)	
	O4	1.494(15)	
	O5	1.565(11)	

Structure Solution of δ-$(MoO_2)_2P_2O_7$. Careful control over the heating rate is crucial for isolation of pure δ-$(MoO_2)_2P_2O_7$. In our hands, the highest purity samples can be prepared by slow heating at 0.33 K/min to 793 K, holding at this temperature for 6 min followed by cooling to room temperature in the furnace. Higher temperatures or more rapid heating led to significant impurities of γ-$(MoO_2)_2P_2O_7$. δ-$(MoO_2)_2P_2O_7$ rehydrates to the precursor material $MoO_2PO_3OH \cdot H_2O$ over a period of several weeks on standing at ambient conditions. High quality room temperature powder diffraction data were indexed to an orthorhombic cell with lattice parameters a = 16.2437 Å, b = 3.8913 Å, and c = 6.2840 Å. Inspection of the systematic absences led to assignment of space group $C222_1$. TGA data supported a molecular formula of $(MoO_2)_2P_2O_7$, and comparison of unit cell volumes with the γ-phase led to predicted unit cell contents of $Mo_4P_4O_{22}$.

Structure solution by simulated annealing of metal atom positions was initially attempted in space group $C222_1$; however, no sensible solution was obtained. The unit cell symmetry was reduced to *Pcan* and after several thousand cycles of stochastic movement of metal atom sites, followed by full Rietveld refinement of the trial model, a solution with reasonable agreement to the X-ray data was obtained. Simulated annealing was subsequently performed using rigid MoO_6 and PO_4 polyhedra allowed to rotate/translate in space until a good agreement with the experimental data was achieved. Inspection of this preliminary model led to a related model in the original space group $C222_1$, which contained octahedral MoO_6 and corner-sharing P_2O_7 groups, the latter being disordered over two sites.

The structure was subsequently refined using synchrotron X-ray data collected on ID31 at the ESRF and time-of-flight neutron diffraction data collected on the HRPD

(24) Zocchi, F. *Solid State Sci.* **2000**, *2*, 383–387.
(25) Brese, N. E.; O'Keeffe, M. *Acta Crystallogr., Sect. B* **1991**, *47*, 192–197.
(26) Kierkegaard, P.; Westerlund, M. *Acta Chem. Scand.* **1964**, *18*, 2217–2225.
(27) Longo, J. M.; Kierkegaard, P. *Acta Chem. Scand.* **1966**, *20*, 72–78.
(28) Kaiser, U.; Schmidt, G.; Glaum, R.; Gruehn, R. *Zeit. Anorg. Allge. Chem.* **1992**, *607*, 113–120.
(29) Tachez, M.; Theobald, F.; Bordes, E. *J. Solid State Chem.* **1981**, *40*, 280–283.
(30) Dupre, N.; Wallez, G.; Gaubicher, J.; Quarton, M. *J. Solid State Chem.* **2004**, *177*, 2896–2902.
(31) Lim, S. C.; Vaughey, J. T.; Harrison, W. T. A.; Dussack, L. L.; Jacobson, A. J.; Johnson, J. W. *Solid State Ionics* **1996**, *84*, 219–226.

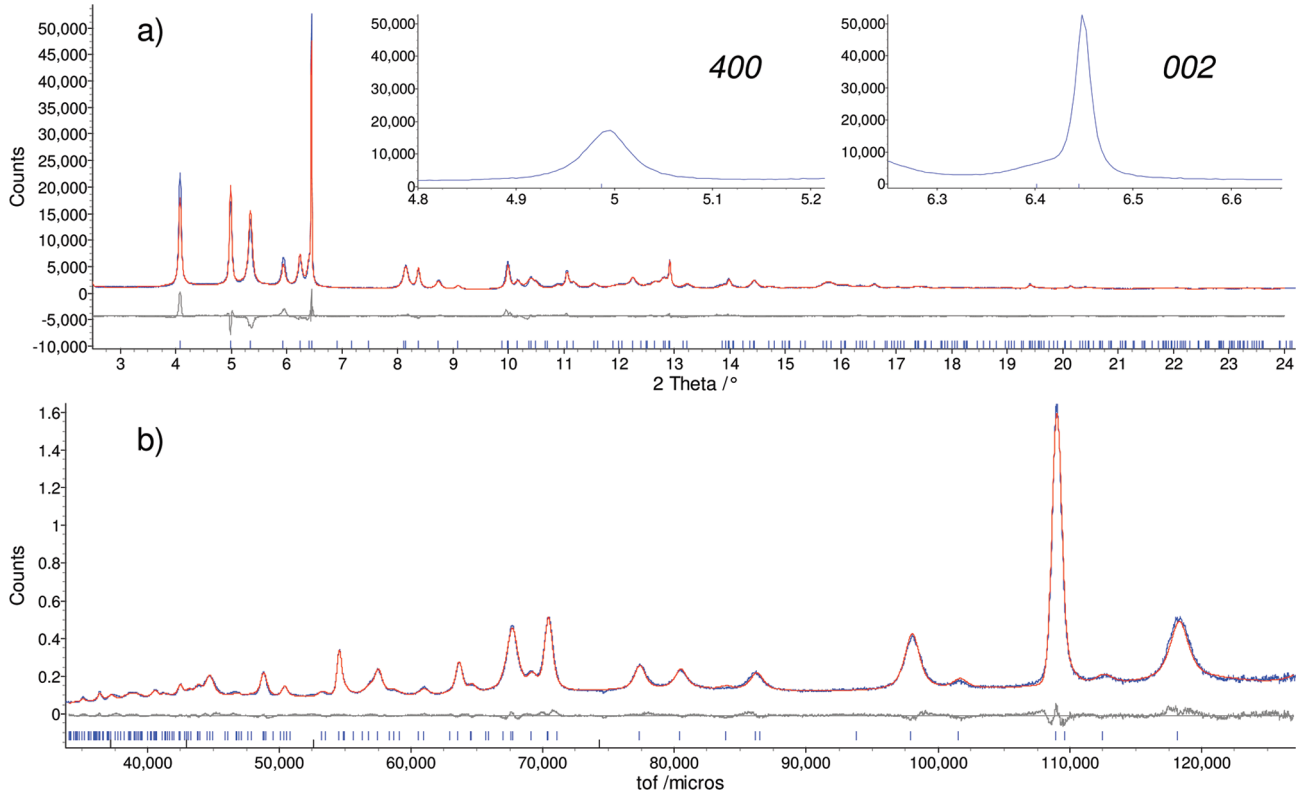

Figure 7. Rietveld fits of δ-$(MoO_2)_2P_2O_7$, against (a) ID31 data and (b) TOF-90° bank data. Insets to panel a show the *hkl* dependence of peakshape. The final overall R_{wp} for these refinements was 4.21%. Individual R_{wp}s for each data set were (a) 8.37 and (b) 3.79%. The figure shows experimental data in blue, calculated pattern in red, and difference plot in gray.

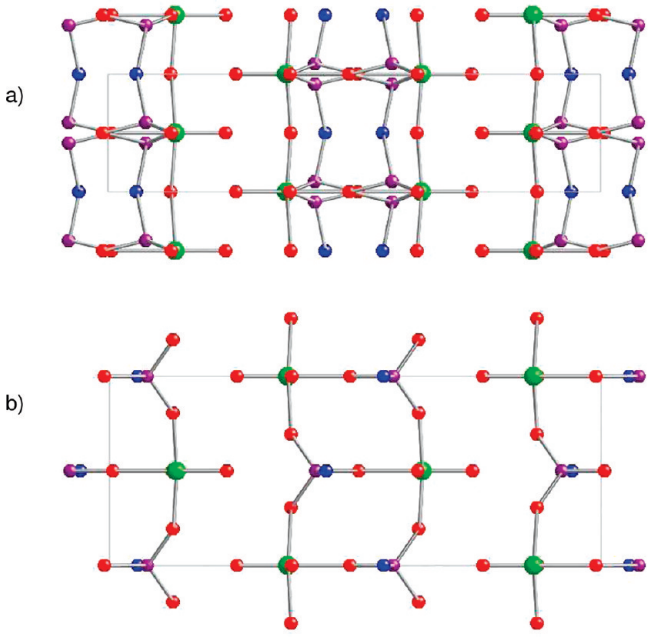

Figure 8. Average structure of δ-$(MoO_2)_2P_2O_7$. Mo atoms are shown in green, P atoms in purple, O atoms in red, and bridging O_b atoms in blue. (a) View down [001]. (b) View down MoO_6 chains along [010]; the P_2O_7 groups link these chains together.

diffractometer of the ISIS neutron source. *00l* reflections were found to be much sharper than other reflections. This *hkl* dependent strain broadening was modeled using the Stephens model.[32] A single function was scaled to both the X-ray and neutron data sets and led to a significant improvement in the quality of the fit. Final Rietveld fits of the 90° neutron and synchrotron data are given in Figure 7. The backscattering data fit is given in the Supporting Information, Figure S6.

Table 3. Selected Refined Values and Crystallographic and Data Collection Parameters for the Combined Synchrotron and Neutron Refinement of δ-$(MoO_2)_2P_2O_7$

space group	$C222_1$	overall R_{wp} (%)	4.21
a (Å)	16.2213(11)	X-ray R_{Bragg} (%)	5.77
b (Å)	3.8936(3)	neutron 90° R_{Bragg} (%)	1.75
c (Å)	6.2772(4)	GOF	3.73
volume (Å^3)	396.46(5)	no. of params	111

Two views of the structure of δ-$(MoO_2)_2P_2O_7$ are given in Figure 8. Selected refinement details are given in Table 3; bond lengths are reported in Table 4; full structural details are given in the Supporting Information in CIF format. The structure is layered along [100] and contains MoO_6 octahedra and PO_4 tetrahedra, the latter linked to form P_2O_7 groups. Each layer is composed of MoO_6 chains along [010] linked by disordered P_2O_7 groups. A short molybdenyl (Mo=O) bond is directed into the layer, two Mo−O vertices link to form Mo−O−Mo chains, whereas the remaining 3 Mo−O vertices link to the three unbonded vertices of each PO_4 tetrahedron. The P atoms and bridging O atoms (shown in purple and blue, respectively, in Figure 8) have an occupancy of 0.5 such that adjacent P_2O_7 units are not simultaneously present.

(32) Stephens, P. W. *J. Appl. Crystallogr.* **1999**, *32*, 281–289.

Table 4. Bond Lengths and Bond Valence Sum Values Calculated for δ-$(MoO_2)_2P_2O_7$; BVSs were Calculated Using R_{ij}[Mo(VI)] = 1.8790 Å,[24] R_{ij}[P(V)] = 1.604 Å, and b = 0.37 Å[25]

central atom	apex atom	bond length (Å)	BVS (vu)
Mo1	O4	1.6687(25)	6.18
	O3	1.9285(24)	
	O3	1.9285(24)	
	O1	1.9516(2)	
	O1	1.9516(2)	
	O2	2.0831(23)	
P1	O2	1.4530(56)	4.98
	O3	1.506(96)	
	O3	1.520(100)	
	O5	1.6364(49)	

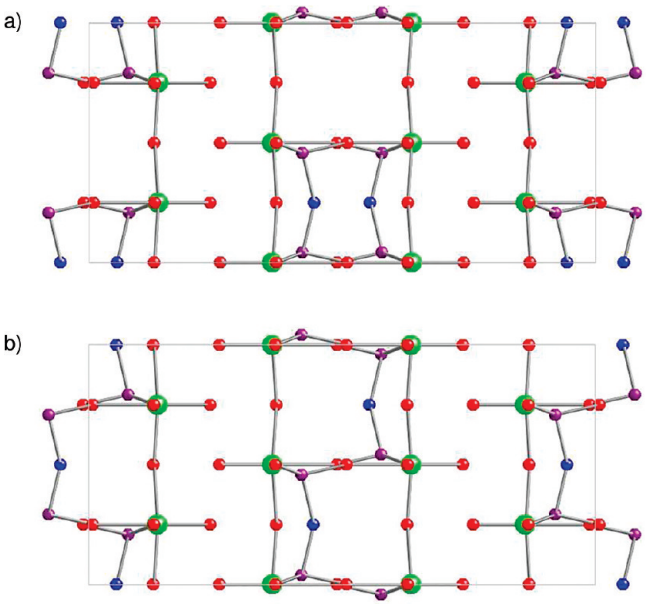

Figure 9. Two possible ordering patterns in δ-$(MoO_2)_2P_2O_7$. (a) The DT1 model, space group $P2$. (b) The DT2 model, space group $P2_1$.

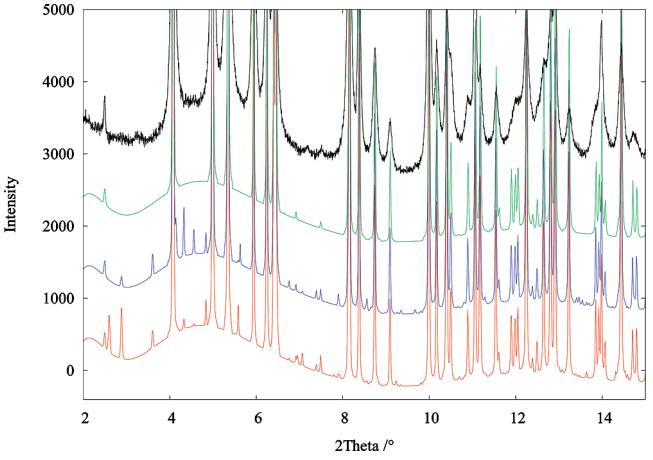

Figure 10. Synchrotron data alongside the simulated patterns of the fully disordered and each of the ordering models for δ-$(MoO_2)_2P_2O_7$; the fully disordered model is plotted in green, DT1 in red, DT2 in blue, synchrotron data in black. The intensity of the strongest peak is 25 000 counts.

The simplest way to remove the disorder in the P_2O_7 groups is to double the b-axis, removing the 2-fold axes

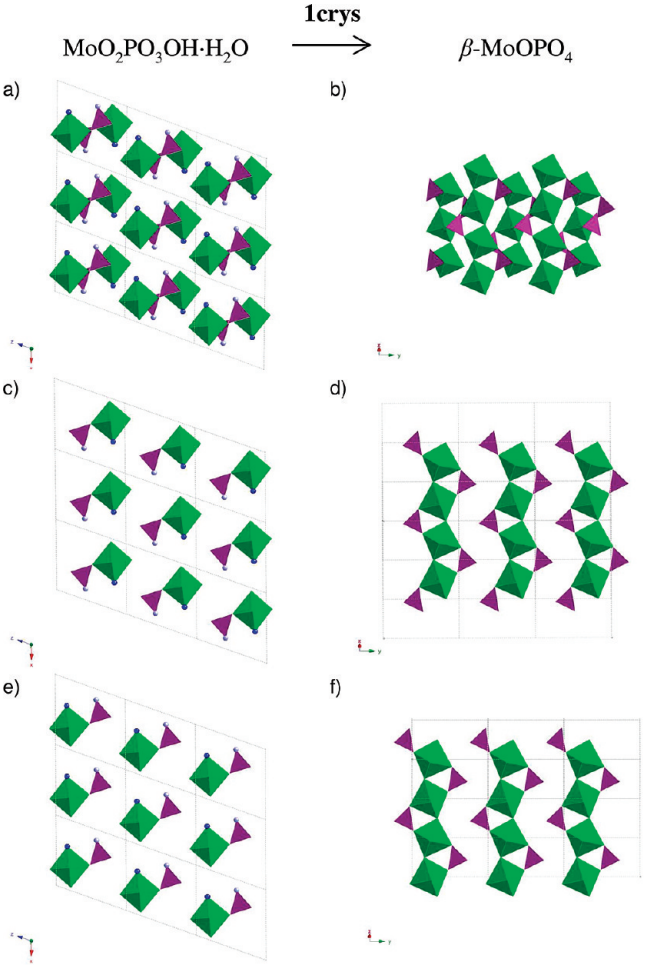

Figure 11. Polyhedral representation of the dehydration from (a) $MoO_2PO_3OH·H_2O$ to (b) β-$MoOPO_4$. (c−f) Single layers within the structures $MoO_2PO_3OH·H_2O$ (c, e) and β-$MoOPO_4$ (d, f) to graphically display the changes that occur on dehydration.

Scheme 2. Phases Observed on Decomposition of $MoO_2PO_3OH·H_2O$; Transformations between Phases Are Labeled for Future Discussion

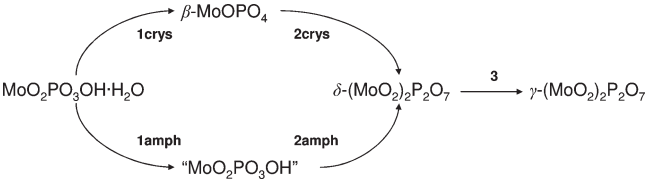

along [100]. Ordering possibilities were investigated using the web-based resource ISODISPLACE.[33] Site occupancy modes DT1 and DT2 influence P and O5 (bridging oxygen) atom occupancies to give ordered models, in space groups $P2$ and $P2_1$ respectively and lead to the two distinct possible ordering patterns shown in Figure 9. An X-ray pattern was simulated for each of these models to compare with the synchrotron data alongside the fully disordered simulation. These patterns are shown in Figure 10. No clear evidence for either ordering pattern can be seen in the experimental data compared to the three simulated patterns.

The observed *hkl* dependent peak broadening is presumably related to short-range P_2O_7 ordering within the material.

(33) Campbell, B. J.; Stokes, H. T.; Tanner, D. E.; Hatch, D. M. *J. Appl. Crystallogr.* **2006**, *39*, 607–614.

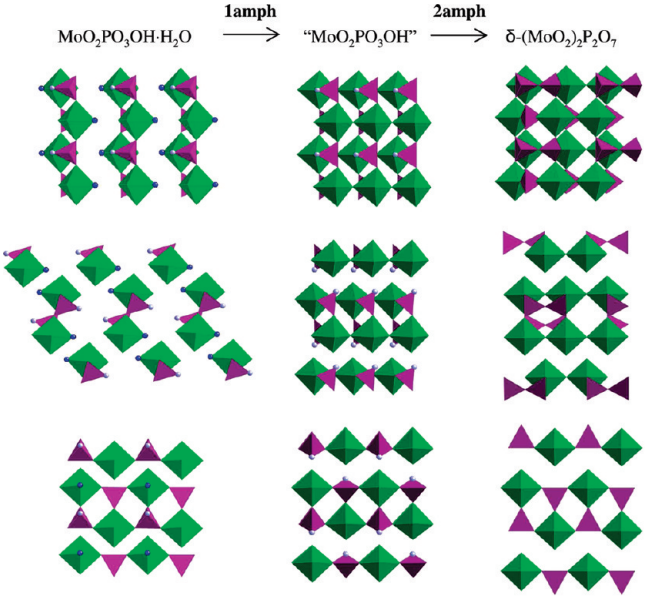

Figure 12. Polyhedral representation of the structures on dehydration from $MoO_2PO_3OH{\cdot}H_2O$ to the hypothetical amorphous MoO_2PO_3OH and δ-$(MoO_2)_2P_2O_7$ (DT1) looking down three sets of related axes in their structures (transformations **1amph** and **2amph**). Mo-centered octahedra are shown in green, P-centered tetrahedra in purple. H atoms are not displayed for ease of viewing. Mo−OH_2 oxygens are given in blue; P−OH oxygens are shown in gray.

We assume that within a given layer the ordering pattern of either 9a or 9b predominates at least locally. However, a relative shift of adjacent layers by a lattice vector b gives rise to an equivalent interdigitation of oxygen atoms, leading to the overall disordered structure observed.

Structural Transformations during the Dehydration. As stated in the introduction, topotactic reactions are typically low-temperature reactions where the crystal structure of a product phase is related to that of a precursor phase. It is interesting to speculate whether topotactic relationships underpin the phase evolution, summarized in Scheme 2, observed in this work.

The formation of the minority crystalline phase β-$MoOPO_4$ (pathway **1crys**) requires loss of water from both $MoO_5{\cdot}H_2O$ dehydration and PO_3OH condensation, reduction from Mo(VI) to Mo(V) and coupled rotations of the polyhedra. Views of the precursor and β-$MoOPO_4$ structures are shown in Figure 11. Panels a and b in Figure 11 are views down 1D MoO_2-$PO_3OH{\cdot}H_2O$ chains in the two structures (the chains are shown in Figures 1 and 12). The MoO_6 chains form (in this view) from condensation of Mo octahedra up the page with an alternating clockwise/anticlockwise tilt of octahedra along the chain direction. Figure 11c−f shows single layers of polyhedra perpendicular to the plane of the paper to illustrate the connectivity changes that occur on dehydration. Figure 11c shows that in the precursor all the PO_3OH groups in this plane are on the left of the octahedra that will form the 1D chains; however, following the transformation, they now sit on both the left and the right (d). Presumably, as two octahedra cross-link, one of the linked PO_3OH groups forms a bond with the second octahedron, which breaks its bond to the initially

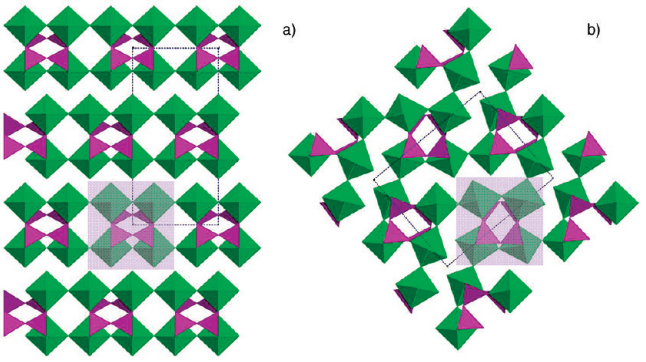

Figure 13. Comparison of the structures of a) δ-$(MoO_2)_2P_2O_7$ (DT1) and b) γ-$(MoO_2)_2P_2O_7$.

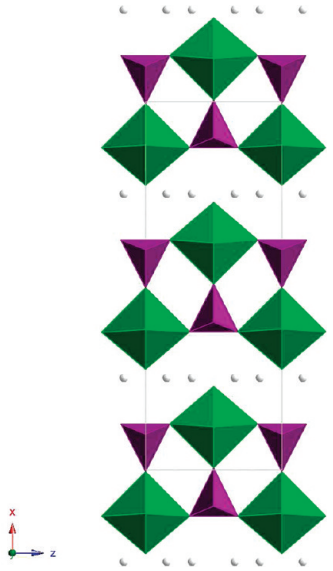

Figure 14. The structure of δ-$Li_x(MoO_2)_2P_2O_7$ showing the Li positions as gray circles.

bound PO_3OH group. This second PO_3OH group then "switches" to bonding to an MoO_6 group in an adjacent forming chain. Panels e and f in Figure 11 show that the opposite behavior occurs in the layer below. This overall transformation requires relatively minor movements of the metal centers relative to each other, suggesting a topotactic transformation. The phase remains only over a small temperature range and we presume it forms only under these kinetically controlled conditions.

The second transformation (**2crys**) is a reconstructive transformation. In β-$MoOPO_4$ all the polyhedra are fully corner-shared with each PO_4 group forming 4 P−O−Mo bonds and each MoO_6 octahedra forming the 4 reciprocal Mo−O−P bonds and 2 Mo−O−Mo bonds along the chains. To transform to δ-$(MoO_2)_2P_2O_7$ one Mo−O−P bond must break allowing formation of a P−O−P linkage and a free molybdenyl Mo═O bond. Quantitative data in Figure 3b suggest that **2crys** is a crystalline-to-crystalline transformation.

Figure 12 shows views of the precursor MoO_2-$PO_3OH{\cdot}H_2O$, a hypothetical model for the amorphous phase $MoO_2{\cdot}PO_3OH$ and δ-$(MoO_2)_2P_2O_7$ to highlight the close structural relationship between them. In the first

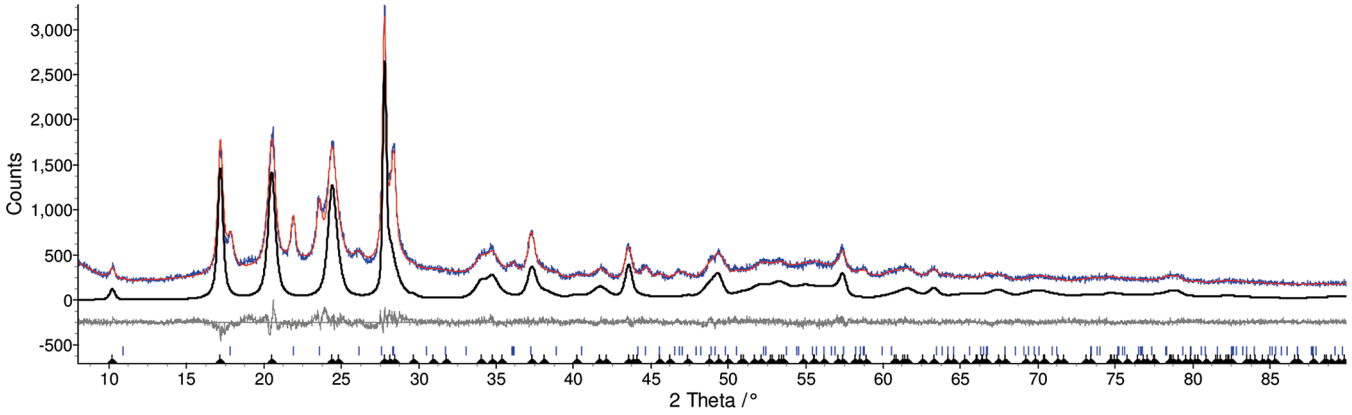

Figure 15. Rietveld fit of the structure refinement of δ-$(MoO_2)_2P_2O_7$ and δ-$Li_x(MoO_2)_2P_2O_7$, with the intercalated phase highlighted in black. This phase formed ~75% of the phase mixture. The final overall R_{wp} for this refinement was 6.50%.

step (**1amph**), we believe the proportion of the precursor that does not transform to β-$MoOPO_4$ (~75% of the total) undergoes condensation of the Mo−OH_2:O−Mo groups in adjacent MoO_6 double chains (Figure 12a) to lose H_2O and give trans, corner-sharing MoO_6 octahedra. We suggest the 1D chains of the precursor thus become cross-linked to form a layered material. A view looking down on these layers is shown at the top of Figure 12, side on views below. This reaction occurs from the relatively low temperature of ~423 K and TGA data suggest a gradual transformation, perhaps with initial loss of H_2O bound to Mo followed by later condensation of P−OH groups. The reaction requires very little movement of the chains relative to each other, consistent with the reaction being topotactic in nature. The amorphous product formed has been found to rehydrate to the starting hydrated phase, $MoO_2PO_3OH \cdot H_2O$; this is further evidence for a close structural relationship.

Complete condensation of the PO_3OH groups within the layers (**2amph**) leads to the formation of the layered phase δ-$(MoO_2)_2P_2O_7$ at 700 K. The pathway proposed would allow for the formation of either the DT1 or DT2 ordering models; they merely arise from a differing relative pairing of the P_2O_7 groups on condensation (Figure 12 middle).

The final transformation (**3**) involves an irreversible reconstructive phase transition from δ-$(MoO_2)_2P_2O_7$ to γ-$(MoO_2)_2P_2O_7$, Figure 13. The two structures have the same empirical formula; both contain chains of MoO_6 octahedra that are linked by P_2O_7 groups, but differ in their relative connectivities. δ-$(MoO_2)_2P_2O_7$ adopts a layered structure with the MoO_6 octahedra corner-sharing via trans linkages; γ-$(MoO_2)_2P_2O_7$ has a 3D structure following the replacement of 50% of the trans linkages with cis linkages, thereby introducing a zigzag pattern to the octahedral chains.

Comparison of the two structures gives some understanding of the driving force behind this transformation. First the difference in volume between the two species at high temperature shows γ-$(MoO_2)_2P_2O_7$ is ~4% larger by volume. The second consideration comes from the values of the P−O−P bond angles within the two structures. Many phase changes are known to occur in phosphate materials to reduce the bond angles in the pyrophosphate groups to an energetically favorable one. In the δ-$(MoO_2)_2P_2O_7$ species the P−O−P bond angle is 154.93(40)° compared to 150.2(5)° in the γ- species. The latter is closer to the expected value of 145° from calculations[34] and 142° (α-$(MoO)_2P_4O_{13}$)[35] and 145.6° (ZrP_2O_7)[36] from experimental observations in other well-characterized phosphates. The structure and phase transitions of γ-$(MoO_2)_2P_2O_7$ that occur on cooling are considered in more detail in elsewhere.[10]

Intercalation Reactions of δ-$(MoO_2)_2P_2O_7$ and γ-$(MoO_2)_2P_2O_7$. Reactions of δ-$(MoO_2)_2P_2O_7$ with ^{n}Bu-Li were carried out to investigate the possibility of intercalation into the layered structure. A notable color change from light gray to black occurred, suggesting the reduction of Mo^{VI} ions. Powder X-ray diffraction data recorded on the resultant powder indicated both the reflections from the layered δ-$(MoO_2)_2P_2O_7$ phase as well as new reflections at higher *d*-spacings which were assigned to an intercalated phase, δ-$Li_x(MoO_2)_2P_2O_7$. Rietveld analysis of the new intercalated phase was initially performed using an expanded parent structure and bond length and angle restraints. Fourier mapping of the powder diffraction data suggested a tentative Li site with tetrahedral oxygen coordination between the layers (Figure 14). Examination of cell parameters revealed an increase in *a* of 1.1 Å and more modest changes in *b*/*c* of −0.16 and +0.14 Å respectively for the intercalated phase, consistent with Li adopting a site between the polyhedral layers. Rietveld analysis with both the unintercalated and the new intercalated model gave the fits shown in Figure 15, with a final R_{wp} of 6.50%. Refinement details are given in Table 5 with further structural details given in Supporting Information in CIF format. Quantitative information was obtained from Ion Beam Analysis experiments on several samples of δ-Li_x-$(MoO_2)_2P_2O_7$. The most crystalline samples had an average Li content of $x = 1.11(8)$.

(34) O'Keeffe, M.; Domenges, B.; Gibbs, G. V. *J. Phys. Chem.* **1985**, *89*, 2304–2309.
(35) Lister, S. E.; Evans, I. R.; Evans, J. S. O. *Inorg. Chem.* **2009**, *48*, 9271–9281.
(36) Stinton, G. W.; Hampson, M. R.; Evans, J. S. O. *Inorg. Chem.* **2006**, *45*, 4352–4358.

Table 5. Selected Refined Values and Crystallographic and Data Collection Parameters for the Structural Refinement of δ-$Li_x(MoO_2)_2P_2O_7$; BVSs were Calculated Using R_{ij}[Mo(V)] = 1.8790 Å,[24] R_{ij}[P(V)] = 1.604 Å, and b = 0.37 Å.[25]

space group	$C222_1$	overall R_{wp} (%)	6.50
a (Å)	17.3171(38)	intercalate R_{Bragg} (%)	1.83
b (Å)	3.7301(8)	no. of structural params	33
c (Å)	6.4173(12)	Mo BVS (vu)	5.69
volume (Å^3)	414.51(15)	P BVS (vu)	5.57

The oxidation state of Mo in δ-$Li_2(MoO_2)_2P_2O_7$ would be +5. The calculated bond valence sum for Mo changes slightly from the unintercalated material, reducing from 6.18 to 5.69, though restraints were used to model the intercalated phase to retain the overall structure. We note one short P−O3 bond length leads to the higher than expected value for the P BVS. These data are given in the Supporting Information, Table S1.

Intercalation reactions were also attempted on γ-$(MoO_2)_2P_2O_7$, but no crystalline intercalated phases were isolated.

Conclusions

Investigation into the dehydration reaction of $MoO_2PO_3OH \cdot H_2O$ has led to the discovery of two new phases en route to γ-$(MoO_2)_2P_2O_7$. A whole powder pattern approach was used to extract quantitative information from VT data, without knowledge of the cell parameters or atomic structures of the new phases. This peak fitting approach allowed optimal conditions to be found to isolate the new phases: β-$MoOPO_4$ and δ-$(MoO_2)_2P_2O_7$. Their structures have been determined from powder diffraction data and a mechanism for the dehydration reaction has been proposed that is consistent with all experimental information available.

The new layered phase δ-$(MoO_2)_2P_2O_7$ has been shown to undergo Li intercalation. The structure of the intercalate has been studied and is consistent with Li^+ ions in sites between the layers, with a 1.1 Å increase in the a cell parameter.

Acknowledgment. We acknowledge EPSRC under EP/C538927/1 for funding. SEL thanks Durham University for a Doctoral Fellowship. We thank the STFC for access to ISIS and ESRF facilities. We thank Irene Margiolaki at the ESRF, Richard Ibberson at HRPD and Ivana Evans for assistance with data collections; we thank Ron Smith for GEM Xpress access. We thank Richard Thompson for the Ion Beam Analysis and Douglas Carswell for the TGA experiments.

Supporting Information Available: X-ray crystallographic files in CIF format for the new structures β-$MoOPO_4$, δ-$(MoO_2)_2P_2O_7$, and δ-$Li_x(MoO_2)_2P_2O_7$. Full details of refined parameters for the whole powder pattern analysis; full listing of the parameters used for the structural refinement of β-$MoOPO_4$; graphs showing the calculation of the amorphous phase percentage from spiking experiments with anatase; full listing of the parameters used for the structural refinement of δ-$(MoO_2)_2P_2O_7$; structural refinement parameters for the intercalated phase δ-$Li_x(MoO_2)_2P_2O_7$. Observed data patterns for each of the four regions of the dehydration reaction. Graphs showing the results from both the whole powder pattern/full Rietveld VT work carried out with a final temperature of 773 K; IR spectra for materials obtained in each of the four regions under study; full details of refined parameters for the Rietveld VT analysis; Rietveld plots for each refinement not given in the paper; bond lengths and bond valence sums calculated for δ-$Li_x(MoO_2)_2P_2O_7$ (PDF). This material is available free of charge via the Internet at http://pubs.acs.org.